Technologies and Materials for Renewable Energy, Environment & Sustainability

Bismuth-Doped Modifications in the Aluminum Antimonide Thin Films Solar Absorber Layers

AIPCP25-CF-TMREES2025-00036 | Article

Bismuth-Doped Modifications in the Aluminum Antimonide Thin Films Solar Absorber Layers

Bushra H. Hussein[1, a)], Bushra K.H. Al-Maiyaly [1, b)], Hanan K. Hassun [1, c)], Ebtisam M-T. Salman [1, d)], Kareem A. Jasim [1, e)] and Auday H. Shaban [2, f)]

[1] *Department of Physics, College of Education for Pure Science (Ibn Al-Haitham), University of Baghdad, Baghdad, Iraq.*
[2]*Department of Remote Sensing & GIS, College of Science, University of Baghdad, Baghdad, Iraq.*

[a)] *Corresponding author: boshra.h.h@ihcoedu.uobaghdad.edu.iq*
[b)] *boshra.k.h@ihcoedu.uobaghdad.edu.iq*
[c)] *hanan.k.h@ihcoedu.uobaghdad.edu.iq*
[d)]*ibtisam.m.t@ihcoedu.uobaghdad.edu.iq*
[e)] *kareem.a.j@ihcoedu.uobaghdad.edu.iq*
[f)] *auday.h.s@ihcoedu.uobaghdad.edu.iq*

Abstract. AlSb: Bi films, which serve as a great absorber layer for the thin-film solar cell, were deposited on many different substrates by the thermal evaporation deposition (TED) method. The physical properties of AlSb thin film were studied. The XRD pattern shows that pure AlSb and Bi-doped AlSb have a polycrystalline cubic structure at room temperature, with a preferential orientation along the (111) plane. The effects of Bi-doped AlSb on the direct band gap of the thin film was understandable (1.78-1.52) eV. The result of the electrical calculation showed that the energy of activation of AlSb: Bi had several low values and high conductivity. AlSb is a promising absorber layer, offering low cost and acknowledged for its great tunable bandgap, with high optical absorption and the use of earth-abundant elements.

Keywords: AlSb: Bi, III-V Semiconductor materials, Bi-doped AlSb, thin film.

INTRODUCTION

Semiconductor material Aluminum Antimonide (AlSb) is a binary compounds, Al and Sb are rich in terrestrial resources and non-toxic ones [1]. III-V compound's semiconductors are great stoichiometric compounds found through combining groups are III elements (In, Al, Ga) & V elements (As,N, P, Sb) [2]. AlSb is a promising modern photoelectric material of conversion that is cost-effective and environmentally benign, aligning well with the solar spectrum, and is considered a viable candidate for the absorber layer in solar cells[3]. AlSb finds application in solar cells because has a higher band-gap as compared with other compounds likes GaSb and InSb [4,5]. Various procedures can be used for deposition AlSb thin film, vacuum evaporation technique [1,6]. co-evaporation technique [7] pulsed laser deposition [8] sputtering of magnetron [9] hot-wall epitaxy [10] electrodeposition [11] chemical vapor [12] molecular beam epitaxy (MBE)[13], one- step facile PLD method [14] AlSb a high efficiency solar materials and high energy gap is potentially, P-type and N-type and of semiconducting in nature [5,15]. The films have high charge carrier mobility, P-conductivity [16]. cubic structures [8]. Numerous researches has looked at the effects of various doped materials on the characterization of AlSb such as the influence of (Zn) doping [14], AlInSb thin films with In content ratios (0.0, 0.1 & 0.3) [5] Cu and Si doping optoelectronic devices [15] AlSb: doped Cu thin film and annealing at different temperatures [3].

This study details the fabrication of Bi-doped AlSb films by the vacuum evaporation approach utilizing bismuth and aluminum-antimony alloying. The physical properties (optical, structural, electrical and I-V characteristics) of those films, were examined. The literature review indicates that there has been no investigation on the impact of Bi-doping on manufacturing of thin film solar cells.

EXPERIMENTAL

A thin film of aluminum and antimony alloy have been manufactured. The stoichiometric weight ratios (1:1) and high elemental purity (99.99%) of the AlSb elements were combined with total quantity of 2 g. The resulting alloy was subjected to a pressure of $6x10^{-3}$ mbar in a quartz tubes, followed by six hours of heating in an electric oven at 1100 K. It should be noted that the temperature necessary to fully solidify the alloy surpasses the melting points of both aluminum and antimony [17]. For the purpose of investigating the optical and structural properties of AlSb and Bi-doped AlSb thin film with ratios (1 and 3)%, they were the material is applied onto glass substrates. at a relative humidity (RT) of $8 x10^{-5}$ Torr in order to produce a 300 nm thin film with good uniformity, adhesion to the substrate, and absence of cracks. The samples were analyzed using several techniques: X-ray diffraction , AFM have characterized have been utilized to define the structural morphology of AlSb and Bi-doped AlSb film. The structure of these films was investigated using X-ray diffraction & Scherer's Formula was employed to calculate their crystalline dimension[18,19].

$$C.S = \frac{0.9\lambda}{B cos\theta} \quad (1)$$

β *denotes* the diffraction width of the peak at half maximum, crystallite size (C.S), (θ) is the diffraction peak angle. Formula for crystal plane spacing in cubic crystalline phase structure [20]:

$$\frac{4sin^2\theta}{\lambda^2} = \frac{h^2 + k^2 + l^2}{a^2} \quad (2)$$

Where Miller incidents (hkl). The calculation of (Ɛ) macrostrain for manufactured thin film can be determined using the following:

$$\varepsilon = \frac{\beta \cos\theta}{4} \quad (3)$$

The density of dislocations (δ) is the ratio of the lengths of dislocation line to the crystal volume. It can be computed using the following [21]:

$$\delta = \frac{1}{(C.S)^2} \quad (4)$$

To determine the energy gap, Measurements of optical transmission within the 400–1000 nm wavelength rang were performed. The optical characteristics of the thin film preparation have been observed through transmission and absorption spectra spanning a wavelength range of 400 to 1000 nanometers. The energy gap (Egopt) has been calculated from the absorption spectrum using the Tauc equations and, Lambert's law, respectively [22,23]:

$$\alpha = 2.303\frac{A}{t} \quad (5)$$

$$\alpha h\upsilon = D\,(h\upsilon - Eg)^r \quad (6)$$

The absorption coefficient is denoted by the symbol (α). The exact values of the temperature-dependent constant (D) and (hυ) signify the magnitude of the photons' incident energy, while the factor r specifies the type of optical transition and the thickness (t).

The refractive index (n) of AlSb:Bi was computed utilizing the Herve-Vandamme relation shown in Eq. (7) [24], expressed as

$$N^2 = 1 + [A/Eg + B]^2 \quad (7)$$

A , B are constants valued at 13.6 eV and 3.4 eV, respectively, while Eg denotes the bandgap.

RESULT AND DISCUSSION

Structural Properties

X-ray diffraction apparatus was employed to obtain crystal structure data of AlSb films. Fig. 1 illustrates that the AlSb film synthesized at room temperature has a polycrystalline structure in the cubic phase, consistent with the reference values in the ICDD 00-006-0233 card. As the Bi doping ratio escalates from 1% to 3%, the AlSb films exhibit enhanced crystallinity. Four diffraction peaks are observed in both pure AlSb films and Bi-doped variants. These peaks are at $2\theta \approx 25.14$ with the (111) preferred orientation due to its reflection peak at intensity being the most pronounced among those peaks and other peaks appearing at 2θ values which equal to 29.09, 41.6, and 49.21 in the X-ray pattern of diffraction, corresponding to (200) ,(220) and (311), respectively. When the Bi doping ratio rises to 3%, the intensity of the diffraction peak increases, indicating that Bi atoms act as nucleation sites, promoting the aggregation of atoms from other elements during crystallization. This systematic aggregation improves the physical

characteristics of thin films. The characteristics of X-ray diffraction, interplanar spacing (d), and crystalline size of the AlSb alloy are presented in Table 1.

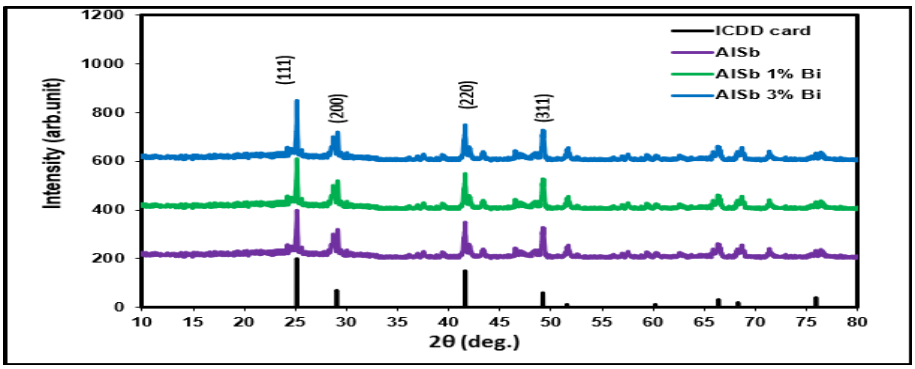

FIGURE 1. X-ray patterns of diffraction the thin film AlSb for standard values in ICDD 00-006-0233 card, pure AlSb grown on the glass substrate and doped with Bi (1% &3%)

The incorporation of Bi at concentrations of 0.01 and 0.03 does not modify the crystalline structures or the orientations of thin films. Nevertheless, the diffraction peaks shift toward higher angles [25-26]. The same table indicates that as the Bi ratio increases to 0.03, the FWHM diminishes until it attains a minimum value of 0.117 degrees, corresponding to a crystal size of 72.67 nm. The results for micro strain and dislocation density have been computed and are presented in Table 1. The lattice constants of AlSb: Bi increased marginally from 6.135 Å to 6.141 Å with a rising Bi doping ratio. The drop in micro strain and dislocation density is apparent as the Bi doping ratio increases. The observed phenomena can be ascribed to the positive correlation between micro-strain and full width (FWHM) at the half maximum of the primary peaks, as well as the negative correlation between dislocation density and crystallite size. The observed reduction in flaws in AlSb: Bi thin films as the doping ratio increases suggests an enhancement in their crystal structure.

TABLE 1. Experimental XRD results for both pure and doped AlSb thin films grown on glass substrates

Thin Film	2θ (Deg.)	d_{hkl}(Å)	hkl	a Å	FWHM (Deg.)	Cs(nm)	δ× 10^{15} (lines/ m^2)	ε*10^{-2}
ICDD card	25.13	3.54	(111)	6.135				
	41.6	2.169	(220)					
AlSb	25.14	3.53	(211)	6.138	0.14770	57.56	0.3018	3.6
	41.6	2.169	(220)					
AlSb: 1% Bi	25.16	3.535	(211)	6.14	0.1380	61.61	0.2634	3.3
	41.8	2.158	(220)					
AlSb: 3% Bi	25.19	3.531	(211)	6.143	0.1170	72.67	0.18	2.8
	42.1	2.413	(220)					

The grain sizes (Average diameter) and Roughness averages of pure AlSb and Bi-doped (1% and 3%) thin films, fabricated via thermal evaporation at room temperature, have been quantified using AFM. The AFM image of AlSb and doped with Bi (1% &3%) thin film are presents in Fig. 2. Table 2 clearly indicates the average particle size and roughness improved trend of increasing (rms) roughness with increasing of Bi doping ratio. Indeed, the grain size increases from 51.56 to 61.26 nm when Bi doping ratio increases from 0 to 3% As Bi doping increased, the surface roughness consistently escalated from 4.22 to 5.39 nm with the increasing of Bi doping. The rougher surfaces for AlSb: Bi films likely originate from Bi atoms, which possess the largest ionic radius (1.17Å) compared to Sb (0.9Å) and Al (0.53Å)[27]. Substituting or incorporating interstitials with a greater size disparity within the crystal structure

results in increased mismatched crystal development. This leads to rougher surfaces due to an increased Bi doping ratio.

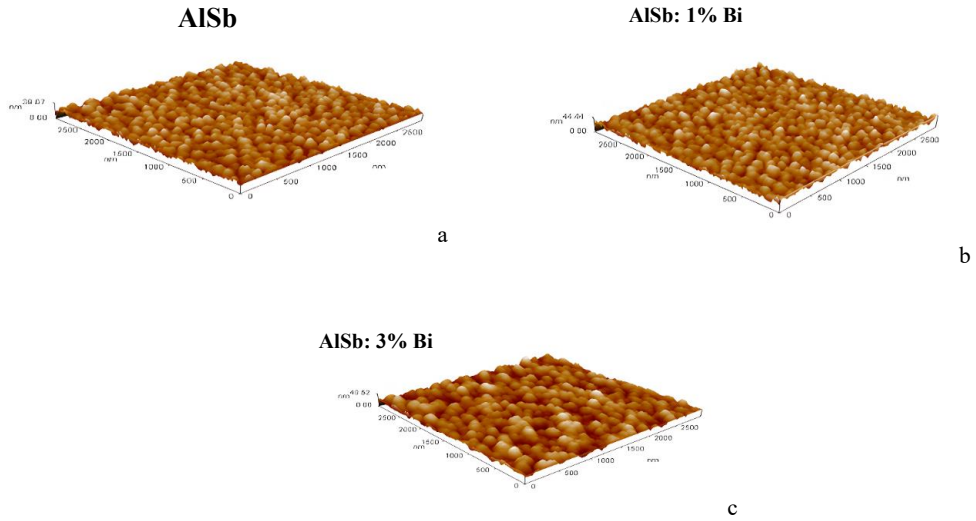

FIGURE 2a,b,c. Three-dimensional atomic force microscopy (AFM) of pure AlSb thin sheets grown on the glass substrate and doped with Bi (1% &3%)

TABLE 2. Roughness average, Average diameter, and the root mean square of pure AlSb grown on the glass substrate and doped with Bi (1% &3%)

Thin Film	Average diameter (nm)	Roughness average (nm)	Root mean square
AlSb	51.56	4.22	5.2
AlSb: 1% Bi	52.61	4.35	5.38
AlSb: 3% Bi	61.26	5.39	6.7

The characteristics of the optical AlSb:Bi thin film was measured via an UV-VIS-NIR spectrophotometer, revealing the optical transmittance spectra within 400 - 1000 nm range, as shown in Fig. 3. Optical transmittance markedly declines as the wavelength diminishes within 700 nm to 815 nm range, which encompasses the absorption edges for AlSb film.

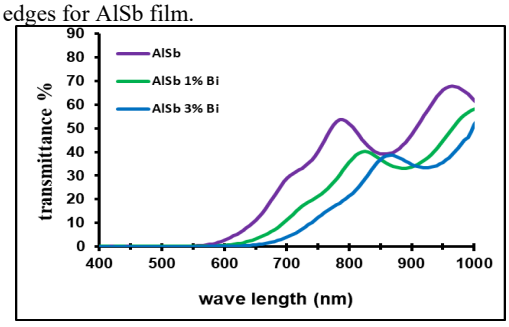

FIGURE 3. The Transmittance spectra of thin pure AlSb and doped with Bi (1% &3%)

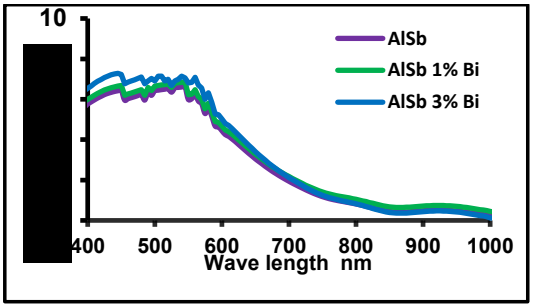

FIGURE 4. The absorption coefficient as a function of wavelength for pure AlSb thin films and those doped with Bi (1% and 3%)

The findings indicate that the undoped AlSb becomes transparent at approximately 700 nm or 1.77 eV, while it absorbs visible light within the 400–750 nm range. With Bi doping, the first positions shift to the longer range.

Nonetheless, all the synthesized AlSb films may serve as suitable materials for the advancement of optoelectronics in response to visible light, given their energy bandgap of 1.78 to 1.52 eV. As we can see from Fig. 5 the absorption spectrum of film distinctly indicates a value exceeding 7.28 * 10^4 cm^{-1} within the wavelength range of 400 nm-600 nm. The values of absorption coefficients about (α>10000 cm^{-1}) indicate that the bandgap is direct, corroborating the findings in [28,29]. The absorption coefficient of these films rises as they near the visible spectrum region, as shown in Fig. 4.

The direct band gap is determined via Tauc equation by the extrapolation of a linear graph, as seen in Fig. 5, for pure AlSb thin films produced on a glass substrate and doped with Bi (1% and 3%). The band gaps are 1.78 eV, 1.65 eV and 1.52 eV correspondingly, as illustrated in Fig. 5. The bandgap of the films varies with varying levels of Bi doping. The influence of various Bi doping levels on the band gap is evident. The bandgap of pure AlSb is 1.78 eV which aligns well with the findings of Ke Yang et al. [8], but for doped Bi, it diminishes to approximately 1.52 eV. The reduced band gap facilitates the absorption of long wavelengths of light when utilized as an absorption layer for solar cells [3,30].

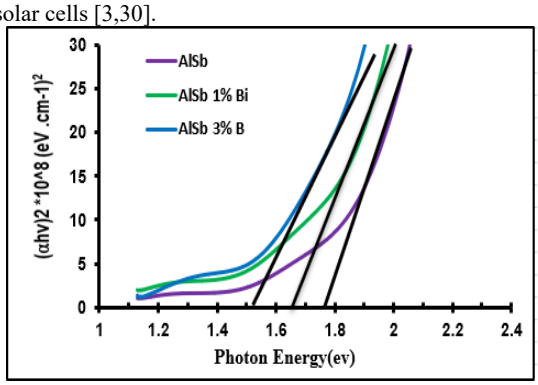

FIGURE 5. (αhυ)² vs photon energy of thin pure AlSb and doped with Bi (1% &3%)

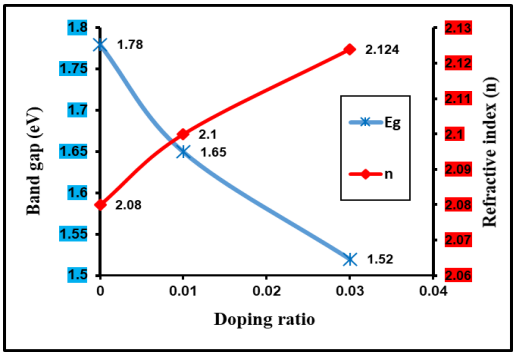

FIGURE 6. The bandgap & refractive index with doping ratio of thin films pure AlSb and doped with Bi (1% &3%)

The alterations in bandgap (Eg) and refractive index (n) computed using the Herve-Vandamme relation for Bi-doped samples (1% and 3%) are illustrated in Fig. 6. The refractive index (n) rises from (2.08) to (2.124) as Bi doping increases. Variations in (n) can be attributed to differences in packing density and the polarizability of the surrounding field [24].

The electrical properties of undoped AlSb and Bi-doped (1% and 3%) thin films play a crucial role in determining the efficiency of these solar cells, particularly in the context of polycrystalline semiconductor films. Electrical conductivity in semiconductors measures the ability of a semiconductor material to conduct electric current, and it is greatly affected by the temperature, impurities, defects, external electric field, and illumination[31].

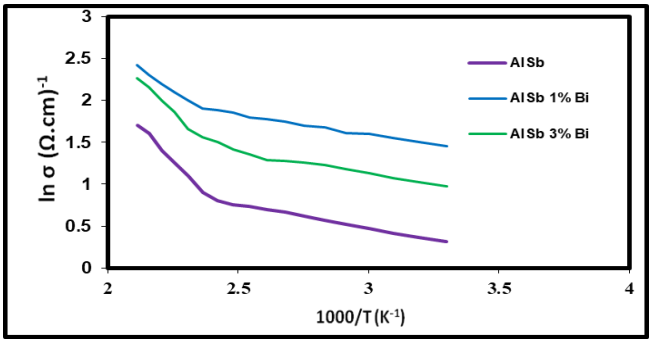

FIGURE 7. ln(σ) vs 1000/T curves of thin film pure AlSb and doped with Bi (1% &3%)

For most cases of semiconductors, the exponential change in (D.C) electrical conductivity with absolute temperature (T) can be given by the Arrhenius equation [32-34]. To studying the conductivity mechanisms of prepared

films, we draw a relationship between (lnσ) and (103/T) as in Fig. (7), we found two D.C conductivity mechanism with two activation energies throughout the temperature range (300-475) K. The initial activation energy Ea1 at low temperatures (300-415 K) arises from carrier transport to some localized states adjacent to the bands of valence and conduction, as well as hopping among confined levels in the energy gap. The subsequent activation energy (Ea2) manifests at elevated temperatures (425-475 K) as a result of the conduction of carriers excited into extended state beyond the mobility edges through thermal excitation. The conductivity rises when the activation energy (Ea) diminishes, which can be attributed to a growth in mobility and carrier concentration [35]. This tendency is attributed to the rise in crystallin size, as indicated by the XRD data. The activation energy value decreases with increasing Bi doped (1% &3%) as in Table (3), i.e., to acceptor levels within the energy gap near the valence [36,37].

TABLE 3. D.C parameters for pure AlSb and doped with Bi (1% &3%)

Thin Film	$\sigma(\Omega.cm)^{-1}$	E_{a1}(eV)	Range of temperatures (K)	E_{a2}(eV)	Range of temperatures (K)
AlSb	1.37	0.277	300-415	0.048	425-475
AlSb: 1% Bi	2.65	0.252	300-415	0.046	425-475
AlSb: 3% Bi	4.06	0.176	300-415	0.041	425-475

CONCLUSION

AlSb: Bi (1% &3%) have been prepared by means of Bismuth and aluminum-antimony alloying by thermal evaporation method. The films pure AlSb and doped with Bi (1% &3%) were polycrystalline It was concluded that crystallization was optimal when doped with 3% Bi, as determined by the combination of XRD and AFM analyses. At the optimum doping of AlSb: 3% Bi, the tow activation energies of AlSb: Bi films was 0.176& 0.041 eV and the band gap for AlSb: Bi 3% film was 1.52 eV. Furthermore, the phenomenon may result from the diffusion of Bi atom and their homogeneous distribution inside the thin film. Absorption coefficient also increased which makes all of them suitable thin films for electro-optical applications, especially for solar cell.

REFERENCES

1. Y. Ch. Sharma, A. Purohit and Y. K. Vijay, International Journal of Innovations in Engineering and Technology **7**, 271-277 (2016).
2. K. Y. Cheng, *III–V Compound Semiconductors and Device* (Springer Nature Switzerland AG, 2020).
3. Y. Pei, H. Yan , R. Xiao, B. Li, K. Yang and H. Song, Vacuum **177**, 1-6 (2020).
4. K. Lal, A. K. Srivastava, S. Singh and R. Kishore, Journal of Materials Science Letters **22**, 515– 518 (2023).
5. Z El. Merzouki, E. Benhsin and M. Cherraj, Bull. Chem. Soc. Ethiop. **4**, 297-304 (2024).
6. S. M and V. YK, Applied Surface Science **239**, 79-86 (2004).
7. Y. Feifei, L. Zhi, F. Lianghuan, Z. Jingquan, L. Wei, and W. Lili, Chin. J. Semicond **27**, 1578–1581 (2006).
8. K. Yang, B. Li, J. Zhang, W.Li, L. Wu, G. Zeng, W. Wang, C. Liu and L. Feng, Superlattices and Microstructures **102**, 1–6 (2017).
9. Z. Huang, L. Wu, B. Li, X. Hao, J. He, L. Feng, W. Li, J. Zhang and Y. Cai, Chin. Phys. B **19** (2010).
10. T. Singh and R.K. Bedi, Thin Solid Films **312**, 111–115 (1998).
11. A. J. Haider, R. H. Al-Anbari, G. R. Kadhim, and C. T. Salame, Energy Procedia 119, 332–345 (2017).
12. M. Leroux, A. Tromson-Carli, P. Gibart, C. Vérié, C. Bernard and M.C.Schouler, J. Cryst. Growth **48**, 367–378 (1980).
13. Jasim, K.A., Journal of Superconductivity and Novel Magnetism, 2013, 26(3), pp. 549–552.
14. P. Tang, W. Wang, B. Li, L. Feng and G. Zeng, Coatings **9**, 1-9 (2019).
15. Abdulateef, A.N., Alsudani, A., Chillab, R.K., Jasim, K.A., Shaban, A.H., Journal of Green Engineering, 2020, 10(9), pp. 5487–5503.
16. Ahmed, B.A., Mohammed, J.S., Fadhil, R.N., ...Shaban, A.H., Al Dulaimi, A.H., Chalcogenide Letters, 2022, 19(4), pp. 301–308.
17. K. Al Abdullah, F. Al Alloush, A. Jaafar, and C. Salame, Energy Procedia 57, (2014).
18. S. N. Sobhi and B. H. Hussein, Ibn Al-Haitham Journal for Pure and Applied Sciences **35**, 16-24 (2022).
19. H. K. Mahmood and B. H. Hussein, Ibn Al-Haitham Journal for Pure and Applied Sciences **38**, 45-54 (2025).
20. H. P. Klug and L. E. Alexander, *X–ray diffraction procedure* (John Wiley & Sons, New York, 2006).

21. R. H. Athab and B. H. Hussein, Chalcogenide Letters **20**, 477 – 485 (2023).
22. S. N. Sobhi and B. H. Hussein, Chalcogenide Letters **19,** 409-416 (2022).
23. B. H. Hussei and H. K. Hassun, NeuroQuantology **18**, 77-82 (2022).
24. L. P. Herve and K. J. Vandamme, Infrared Phys. Technol. **35**, 609–615 (1994).
25. S. N. Sobhi and B. H. Hussein, Journal of Ovonic Research **18**, 519–526 (2022).
26. R. H. Athab and B. H. Hussein, Chalcogenide Letters **20**, 94-100 (2023).
27. N. N. Greenwood and A. Earnshaw, *Chemistry of the Elements*, (Elsevier ,University of Leeds, U.K, 2012).
28. M. H. Mustafa, H. M. Ali, N. F. Habubi and B. H. Hussein, Journal of Materials Science: Materials in Electronics, **35**, 1-8 (2024).
29. R. H. Athab, B. H. Hussein and Sameer A. Makki, "Effect of in on the properties of AlSb thin film solar cell", AIP Conference Proceedings, 2123, 020030-9, 2019.
30. B. K. Al-Maiyaly, B. H. Hussein, A. H. Shaban, "Fabrication and characterization study of ZnTe/n-Si heterojunction solar cell application", IOP Conf. Series: Journal of Physics: Conf. Series 1003, 012084, 2018.
31. H. K. Hassun , B. H. Hussein, B. K. H. Al-Maiyaly, Y. K. H. Moussa, A. H. Shaban, K.A. Jasim, "Impact thickness on performance of higher quality ZnTe photodetectors", AIP Conference Proceedings, 3321, 020018, 2025.
32. L. H. Feng, J. Q. Zhang, B. Li, W. Cai, Y. P. Cai, L. L. Wu, W. Li, J. G. Zheng, Q. Yan, G. P. Xia and D. L. Cai, Thin Solid Films **491**, 104 (2005)
33. Sa. M. Ali, H. K. Hassun, A. A. Salih, R. H. Athab, B. K. H. Al-Maiyaly, B. H. Hussein, Chalcogenide Letters **19**, 663 – 671 (2022).
34. B.B. Kadhim, I.H. Khaleel, B.H. Hussein, K.A. Jasim, A. H Shaban, B K. Al-Maiyaly and Sh. H. Mahdi "Effect of gamma irradiation on the TlBa2Ca2Cu3O9-δ superconducting properties", AIP Conference Proceedings, 1968, 030054, 2018.
35. B. H. Hussein, I. H. Khudayer, B. K. H. Al-Maiyaly, H. K. Hassun, "Study and preparation of optoelectronic properties of AgAl1-xInxSe2/Si heterojunction solar cell applications", AIP Conference Proceedings, 2437, 020032, 2022.
36. A. G. Nilens, *Deep Impurity in Semiconductors*, (Wiley-Interscience Publication, Canada, 1973).
37. B. K. Al-Maiyaly, B. H. Hussein, A. A. Salih, A. H. Shaban, Sh. H. Mahdi and I. H. Khudayer, "Synthesis and characterization study of n-Bi_2O_3/p-Si heterojunction dependence on thickness," AIP Conference Proceedings, 1968, 030046-11, 2018.